Editors' Suggestion

Tomographic Extraction of the Internuclear Separation Based on Two-Center Interference with Aligned Diatomic Molecules

RenPing Sun,[1,2] XuanYang Lai,[1,*] ShaoGang Yu,[1,2] YanLan Wang,[1] SongPo Xu,[1,2] Wei Quan,[1] and XiaoJun Liu[1,†]
[1]State Key Laboratory of Magnetic Resonance and Atomic and Molecular Physics, Wuhan Institute of Physics and Mathematics, Chinese Academy of Sciences, Wuhan 430071, China
[2]School of Physics, University of Chinese Academy of Sciences, Beijing 100049, China

(Received 5 November 2018; published 14 May 2019)

We experimentally investigate the two-dimensional photoelectron momentum spectra of aligned diatomic molecules in an intense laser field. Our results reveal a novel prominent valley structure in the molecular alignment dependence of the high-energy photoelectron spectra along the laser polarization. Resorting to the molecular strong-field approximation and a simple semiclassical analysis, we show that this valley structure stems from the destructive two-center interference of the laser-driven rescattered electrons in diatomic molecules. Based on this two-center interference with aligned diatomic molecules, we demonstrate for the first time a tomographic method to extract the molecular internuclear separation, providing a more straightforward approach of molecular imaging, in comparison with, e.g., laser-induced electron diffraction and fixed-angle broadband laser-driven electron scattering.

DOI: 10.1103/PhysRevLett.122.193202

When subject to an intense laser pulse, an atom or a molecule ionizes. After being ionized, part of the electron wave packet may be driven back and recollide with the parent ionic core when the laser electric field changes sign. This simple electron rescattering mechanism [1,2] governs many strong field atomic and molecular processes such as high-order above-threshold ionization (HATI) [3], high-order harmonic generation (HHG) [4], and nonsequential double ionization (NSDI) [5], and serves as the basis for current attosecond and strong field physics [6].

In comparison with simple atoms, molecular ionization is expected to exhibit a large variety of peculiar effects closely related to its structural complexity and extra nuclear degrees of freedom. One intriguing effect is directly relevant to the multiatomic-center of a molecule: the ionized electron in, e.g., a diatomic molecule may be emitted coherently from the two atomic centers and exhibit an intrinsic interference effect, which is equivalent to the famous double-slit interference. This effect has been previously demonstrated both theoretically and experimentally in, e.g., a pronounced suppression of the total ionization yields as well as the low-energy photoelectron yields of a diatomic molecule of O_2 compared to its companion atom of Xe with a similar ionization potential [7–12].

Alternatively, part of the ionized electron wave packet may return and recollide with different atomic centers, leading to a novel two-center interference of the laser-driven rescattered electron. Indeed, the fingerprint of this novel two-center interference, arising from the quantum nature of the recolliding electron, has been initially predicted theoretically in both HHG and HATI spectra with a model diatomic molecule under different molecular alignment with respect to the laser polarization [13,14]. Preliminary experimental evidence of this interference effect has been found in HHG spectra of an aligned CO_2 molecule [15–17], but interestingly, not in simpler diatomic molecules such as O_2 and N_2, due to their much smaller internuclear distances. In contrast, recent theoretical studies show that this interference effect, which can be described with a simple term, $\cos(\mathbf{q}\cdot\mathbf{R}_0/2)$, may manifest itself in the angle-resolved HATI spectra of aligned N_2 and O_2 molecules [18,19], where $\mathbf{q}$ is the momentum transfer of the rescattered electron before and after the recollision and $\mathbf{R}_0$ denotes the molecular internuclear separation. A following experimental study was performed, however, with randomly oriented molecules of N_2 and O_2, and it was found that a clear destructive interference survives for O_2, but not for N_2 due to the alignment averaging effect [20].

On the other side, based on this two-center interference effect from rescattered electron in HATI, an intriguing molecular imaging method was first proposed more than twenty year ago [21]. Until recently, this so-called laser-induced electron diffraction (LIED) scheme has been successfully employed in probing the molecular structure and ultrafast dynamics (see, e.g., Refs. [22,23]). Note that, however, in this LIED scheme, the extracted photoelectron yield is a function of the momentum transfer $\mathbf{q}$ of the corresponding recolliding electron with different scattering angles upon the two-center target molecules. Thus, the two-center interference pattern is superimposed by the modulations due to the atomic scattering differential cross section (DCS) and *a priori* knowledge of the atomic DCS needs to be derived as a prerequisite [22]. To eliminate some of the

 © 2019 American Physical Society

complexities in LIED, a fixed-angle broadband laser-driven electron scattering (FABLES) scheme was further demonstrated [24,25] by studying the back-rescattered electron with fixed scattering angle but with different recolliding energies. In this scheme, the corresponding two-center interference fringes are entangled with the energy-dependent background signal, that is, atomic scattering DCS and electron returning broadband wave packet. To overcome the disadvantages inherent to LIED and FABLES, an alternative imaging method, for which one may fix the momentum of $\mathbf{q}$ but rotate the molecular internuclear distance of $\mathbf{R}_0$ by employing the molecular alignment technique, may be envisioned. This is essentially a tomographic method and will avoid the complexities with the modulation of atomic DCS in extracting the molecular structure. However, until now, such a tomographic method with aligned molecules has not yet been achieved.

In this Letter, we demonstrate this tomographic method to retrieve the molecular structure with a pre-aligned diatomic molecule N_2. Our measurement shows a prominent valley structure in the alignment dependence of the high-energy photoelectron spectra along the laser polarization direction. In terms of the molecular strong-field approximation (MSFA) theory, this novel valley structure is well reproduced and further simple semiclassical analysis reveals its origin as a direct evidence of the destructive two-center interference from the rescattered electrons. Based on this two-center interference, we show that the detailed information about the molecule, i.e., the internuclear separation, can be extracted directly from the alignment-dependent photoelectron spectra, in the context of tomographic imaging.

The experiment is performed with cold-target recoil-ion momentum spectroscopy (COLTRIMS) [26–28]. The femtosecond linearly polarized laser pulses are generated from a commercial Ti:sapphire femtosecond laser system (FEMTOPOWER compact PRO CE-Phase HP/HR) with a repetition rate of 5 kHz, a pulse duration of around 30 fs, and a center wavelength of 800 nm. The pulse is split into a stretched alignment pulse (~80 fs) and a probe pulse (~30 fs) with variable relative delay. Two pulses are focused by an on-axis spherical mirror ($f = 75$ mm) onto a cold supersonic gas jet inside the COLTRIMS vacuum chamber with the transverse and longitudinal translational temperatures less than 5 and 20 K, respectively. The probe pulse, which is applied after a time delay of about 4.1 ps for N_2 and 5.9 ps for O_2, ionizes the aligned molecules produced by the alignment pulse. Any alignment angle can be achieved by rotating the alignment pulse polarization with a half-wave plate [29]. The alignment degree $\langle\cos^2\vartheta\rangle$ estimated from a 2D angular distribution of ions by using the Coulomb explosion method [30,31] is 0.79 for N_2 and 0.73 for O_2 at the corresponding time delay, respectively. We measure the three-dimensional momenta of the produced photoelectrons in coincidence with the singly charged ions. The alignment pulse creates a low ionization background (<0.5%) compared to the ionization pulses. By fitting the delay-dependent alignment degree [30], we obtain the alignment pulse intensity of about 6.5×10^{13} W/cm^2 for N_2 and the initial rotational temperature of the molecule about 50 K, while for O_2, the alignment pulse intensity is about 3.5×10^{13} W/cm^2 with the rotational temperature of the molecule about 60 K. On the other hand, the laser intensities of the ionization pulses are calibrated with a procedure utilizing the photoelectron momentum distribution in a close-to-circularly polarized laser field [32].

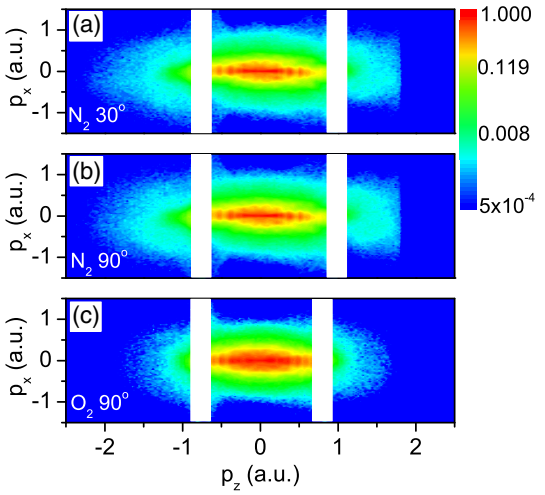

FIG. 1. The measured two-dimensional photoelectron momentum spectra of aligned diatomic molecules. p_z and p_x are the momenta of the electron along and perpendicular to the laser polarization, respectively. (a) For N_2 with the alignment angle $\theta_L = 30°$, (b) for N_2 with $\theta_L = 90°$, and (c) for O_2 with $\theta_L = 90°$. The peak intensities of the laser pulses are 1.2×10^{14} for N_2 and 1.0×10^{14} W/cm^2 for O_2, respectively. The momentum spectra have not been symmetrized, and data points in the white area are removed because of the influence of the spectrometer magnetic field [26,33]. All of the spectra are normalized by 1 at their maxima.

Figures 1(a) and 1(b) present the measured two-dimensional photoelectron momentum spectra of N_2 at the alignment angles of $\theta_L = 30°$ and 90°, respectively. For comparison, we also present the two-dimensional photoelectron momentum spectra of O_2 at $\theta_L = 90°$ in Fig. 1(c). Our measurement shows that in comparison with the spectra of N_2, the electron yields of O_2 in the region with $|p_z| > 1.25$ a.u., which corresponds to the rescattered electrons [3], are significantly suppressed. This phenomenon is closely related to the antibonding symmetry of the valence orbital of O_2 and can be understood as a consequence of the symmetry-induced destructive interference of the electron wave packet during the tunneling ionization [10,18,19]. Because of the extremely low electron yields of O_2 in this high-energy regime, we will focus on the spectra of N_2 and demonstrate the two-center interference of the

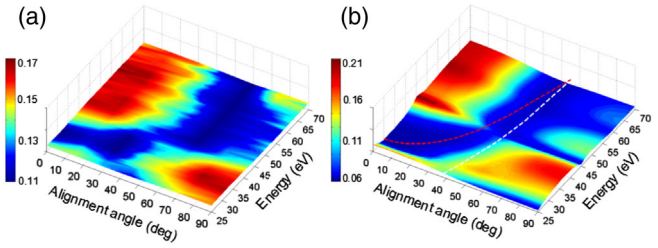

FIG. 2. Density plot of the measured (a) and simulated (b) photoelectron spectra of the back-rescattered electrons in the energy region of 25–70 eV with respect to the molecular alignment angle from 0° to 90°. The two dashed curves in panel (b) are based on the relation of $\cos[(p-k)R_0\cos\theta_L/2]=0$ for the long (red) and short (white) orbits, respectively. For more details, see text.

rescattered electrons, though similar two-center interference also, in principle, imprints in the spectra of O_2.

At first glance, the photoelectron momentum spectra of N_2 in Figs. 1(a) and 1(b) seem to be qualitatively indistinguishable, which is partially due to the imperfect alignment in the experiment and rapid falloff of the high-energy electron yields. However, when we focus on the photoelectrons with the momenta along the p_z axis, corresponding to the back-rescattered electrons [34], as a function of alignment angle, distinct fingerprints arising from the two-center interference of rescattered electrons is uncovered. Figure 2(a) presents the density plot of the photoelectron spectra of the back-rescattered electrons in the high-energy region of 25–70 eV (the ponderomotive energy of the laser pulse $U_p \approx 7.1$ eV [3]), with respect to the molecular alignment. For visual convenience, the yields of the photoelectrons with identical energy have been normalized [35,36]. Interestingly, a prominent valley structure is observed in the photoelectron spectra, which starts from the energy region around 30 eV at $\theta_L = 0°$ and extends up to the higher energy region, e.g., around 70 eV at $\theta_L = 60°$. In order to achieve deep insight into this novel valley structure in the photoelectron spectra, we resort to the simulation with the MSFA theory and a simple semiclassical analysis.

Within the MSFA theory [18,19], the transition amplitude of the photoelectron from the initial bound state ψ_0 of molecule to the final continuum state with momentum $\mathbf{p}$ is given by $M_{\mathbf{p}}^{\mathrm{MSFA}} = M_{\mathbf{p}}^{(0)} + M_{\mathbf{p}}^{(1)}$, where

$$M_{\mathbf{p}}^{(0)} = -i\int_{-\infty}^{\infty} d\tau \langle \mathbf{p}+\mathbf{A}(\tau)|\mathbf{r}\cdot\mathbf{E}(\tau)|\psi_0\rangle \exp[iS_0(\mathbf{p};\tau)] \quad (1)$$

describes the direct ionization amplitude, while

$$M_{\mathbf{p}}^{(1)} = -\int_{-\infty}^{\infty} dt \int_0^{\infty} d\tau \left(\frac{2\pi}{i\tau}\right)^{3/2} V_{\mathbf{p}-\mathbf{k}} \times \langle \mathbf{k}+\mathbf{A}(\tau')|\mathbf{r}\cdot\mathbf{E}(\tau')|\psi_0\rangle \exp[iS_1(\mathbf{p};t,\tau)] \quad (2)$$

with $V_{\mathbf{p}-\mathbf{k}} = \langle \mathbf{p}|V|\mathbf{k}\rangle = \langle \mathbf{p}+\mathbf{A}(t)|V|\mathbf{k}+\mathbf{A}(t)\rangle$ and $\tau' = t-\tau$ is the rescattering amplitude. Here, $\mathbf{A}(t)$ is the laser vector potential, $S_0(\mathbf{p};\tau)$ and $S_1(\mathbf{p};t,\tau)$ are the actions, and $\mathbf{k} = -\int_{\tau}^{t} dt' \mathbf{A}(t')/\tau$ is the intermediate momentum of the liberated electron between ionization and rescattering. The molecular initial state ψ_0, within the fixed-nuclei approximation, can be written as a linear combination of atomic orbitals (LCAO) [37,38], $\sum_a c_a[\psi_a^{(0)}(\mathbf{r}+\mathbf{R_0}/2) + (-1)^{l_a-m_a+|m_a|}\psi_a^{(0)}(\mathbf{r}-\mathbf{R_0}/2)]$, where l_a and m_a are the orbital and magnetic quantum numbers, respectively, and $\psi_a^{(0)}$ is the Slater-type orbital [39]. Moreover, to compare with the experimental measurement, the ionization yield has to be integrated over the spatiotemporal intensity distribution in the laser focus (see, e.g., Ref. [40]) and over the angular distribution of the imperfect molecular alignment [31].

Figure 2(b) shows the density plot of the alignment dependence of the simulated photoelectron spectra along the laser polarization direction in the high-energy region of 25–70 eV. The main features of the photoelectron spectra are well consistent with the measurement. For example, there is a prominent valley structure from the energy region of 30 eV at $\theta_L = 0°$ to the higher energy of 70 eV at $\theta_L = 53°$.

We will now show that the prominent valley structure observed in the high-energy photoelectron spectra is a distinct fingerprint of the destructive two-center interference of the rescattered electrons. When the rescattered electron elastically scatters off the diatomic molecule, the momentum of the electron is changed from the incident momentum $\mathbf{k}+\mathbf{A}(t)$ to the scattered momentum $\mathbf{p}+\mathbf{A}(t)$ and thus, the momentum transfer $\mathbf{q} = [\mathbf{p}+\mathbf{A}(t)] - [\mathbf{k}+\mathbf{A}(t)] = \mathbf{p}-\mathbf{k}$. The rescattering of the electron on the two atomic centers in the molecule forms a two-center interference term in the scattering amplitude [22]

$$e^{i\mathbf{q}\cdot\mathbf{R}_0/2} + e^{-i\mathbf{q}\cdot\mathbf{R}_0/2} = 2\cos(\mathbf{q}\cdot\mathbf{R}_0/2) = 2\cos[(\mathbf{p}-\mathbf{k})\cdot\mathbf{R}_0/2]. \quad (3)$$

For the photoelectron along the laser polarization, $(\mathbf{p}-\mathbf{k})\cdot\mathbf{R}_0/2 = (p-k)R_0\cos\theta_L/2$. Destructive interference occurs when the value of $(p-k)R_0\cos\theta_L/2$ is equal to $(2n+1)\pi/2$ $(n=0,1,2,\ldots)$. In the simple man's model, there are two dominant rescattered orbits for each photoelectron, which are best known as the "long orbit" and "short orbit" [3]. In Fig. 2(b), we plot the interference minima based on the relation of $\cos[(p-k)R_0\cos\theta_L/2] = 0$ for the long and short orbits, respectively. Our simulation shows that the red dashed curve of the long orbit qualitatively provides a perfect fit of the valley structure in the spectra, which clearly indicates that the valley structure stems from the destructive two-center interference of the rescattered electrons. Interestingly, we find that the valley structure in the MSFA simulated spectra is wider than the

prediction of the simple man's model. The main reason is that, in fact, in the MSFA theory [18,19], there is a swarm of the rescattered orbits around the two specific long and short orbits with the same final momentum. These rescattered orbits have the different ionization times τ and the rescattering times t, and hence the different values of k. According to Eq. (3), the corresponding alignment angles of the interference minima are changed accordingly. Therefore, the coherent superposition of the different rescattered orbits leads to the relatively wide interference minima structure in the spectra. Furthermore, our calculation shows that in comparison with these rescattered orbits around the long orbit, the difference of the values of k is much more significant for the rescattered orbits around the short orbit, especially for the low-energy photoelectrons (not shown here). Thus, the change of the corresponding alignment angle of the interference minima is also significant, resulting in the blurring of the interference minima for the short orbit in the low-energy region of the photoelectron spectra. Our result is qualitatively well consistent with the simulated spectra and the measured spectra shown in Fig. 2.

In the following, we will demonstrate that the two-center interference feature in the alignment-dependent photoelectron spectra provides a tomographic method in retrieving molecular structure. According to Eq. (3), the two-center interference of the back-rescattered electron is closely related to the molecular internuclear separation R_0. However, due to the influence of a swarm of the rescattered orbits with different values of k, the two-center interference minima cannot be accurately determined. In this Letter, we propose a simple and straightforward method by reducing the effect of k on the two-center interference. Equation (3) can be expanded as $\cos[(p-k)R_0\cos\theta_L/2]=\cos(pR_0\cos\theta_L/2)+R_0\cos\theta_L\sin(pR_0\cos\theta_L/2)k/2+O(k)^2$. For the laser pulse with, e.g., a short wavelength, the values of p and k decrease [3,34]. If the variable $|pR_0\cos\theta_L/2|$ of the zero-order term in the Taylor expansion is smaller than $\pi/2$, the decrease of the values of p and k results in the increase of the zero-order term and, conversely, the decrease of the other terms. Therefore, the contribution of the zero-order term becomes dominant and the corresponding interference feature in the photoelectron spectra can be safely described with a simple term $\cos(pR_0\cos\theta_L/2)^2$.

Figure 3(a) presents the density plot of the alignment dependence of the measured photoelectron energy spectra along the polarization direction of the laser pulses with a short wavelength of 400 nm, for which the maximal value of $|pR_0\cos\theta_L/2|$ is 1.5 ($<\pi/2$) at the cutoff energy of the spectra with $\theta_L=0$. With increasing θ_L or decreasing the photoelectron energy, the value of $|pR_0\cos\theta_L/2|$ will decrease monotonically, leading to that no valley structure from the two-center interference can be observed in the spectra, which is different from the spectra with 800 nm laser pulse shown in Fig. 2. To more directly show the change of the photoelectron yields with the alignment

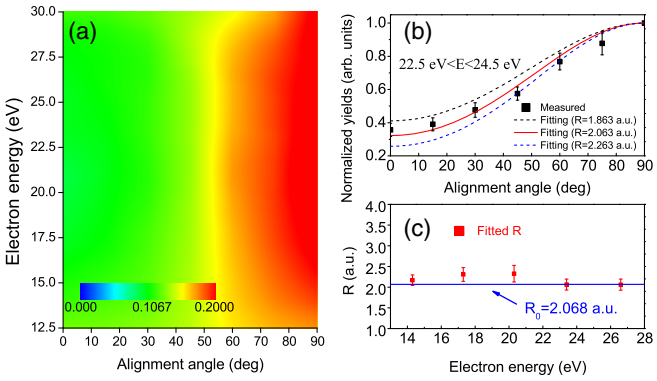

FIG. 3. (a) Density plot of the measured photoelectron spectra along the laser polarization direction with respect to the alignment angle from 0° to 90° with 35 fs, 400 nm laser pulses with peak intensity of 2.0×10^{14} W/cm^2. (b) Extracted electron yields in the energy region of 22.5 eV $< E <$ 24.5 eV with respect to the alignment angle. The error bars represent the standard deviation resulting from experimental uncertainties. The smooth evolution of the yields with the alignment angle is fitted to the interference term $\cos(pR\cos\theta_L/2)^2$. The solid red line is the yield calculated using the best-fit internuclear separation. The dashed black and blue lines are the calculated yields using the internuclear separations of 1.863 and 2.263 a.u., respectively. (c) The retrieved internuclear separations for various photoelectron energies. The error bars denote the error in the fitting with the least square method. The blue line denotes the well adopted internuclear separation of N_2, $R_0=2.068$ a.u..

angle, we extract the photoelectron yields from the measured spectra at different alignment angles. In Fig. 3(b), we present the extracted yields of the photoelectrons in the energy region of, e.g., 22.5 eV $< E <$ 24.5 eV with respect to the alignment angle. The smooth evolution of the yields with the alignment angle is fitted to the interference term $\cos(pR\cos\theta_L/2)^2$. To better compare with the experimental measurement, we also consider the alignment distribution of molecule in experiment [31]. The best-fit is shown as a solid red curve with the fitted value of $R=2.063$ a.u., which agrees well with the N_2 internuclear separation of $R_0=2.068$ a.u. in the literature [39]. For comparison, we also plot in Fig. 3(b) the theoretical yield with the internuclear separations deviating from the fitted value by ±0.2 a.u. Furthermore, we fit the alignment dependence of the photoelectron yields for different energy regions of the spectra and the retrieved internuclear separations are plotted in Fig. 3(c). Our simulations show that the internuclear separations extracted from the measured photoelectron spectra with the simple interference term $\cos(pR\cos\theta_L/2)^2$ qualitatively agree well with the N_2 internuclear separation marked by the blue line in Fig. 3(c).

It is worth noting that, comparing to the well-explored LIED and FABLES schemes [22–25,41,42], our tomographic method exhibits several benefits. First of all, in our method, we explore the back-rescattered photoelectron

with fixed final energy as a function of the alignment angle. The corresponding elastic differential scattering amplitudes of constituting atoms, which are entangled with the two-center interference pattern in LIED and FABLES (see, e.g., Refs. [22,24]), are independent on the molecular alignment and thus, cancel out as a common factor. Second, in our method, the extracted electron-ion DCSs can be described with a simple two-center interference term $\cos(pR\cos\theta_L/2)^2$, which is directly related to the measured photoelectron momentum **p**, while in LIED and FABLES, a relatively complicated derivation of the relation between the scattering momentum and the measured momentum of the photoelectron has to be taken [22–24]. Last but not least, in our method, the entire high-energy photoelectron spectra with high yields can be safely used to retrieve the information of the molecular internuclear separation, while the LIED method usually selects the highest energy photoelectrons in the spectra to diminish the contamination from other rescattered orbits, with the cost of the relatively low photoelectron yield. To improve the experimental efficiency in LIED, the DCS with the lower energy photoelectrons is used with a plausible assumption that the contribution of the long orbit dominates in the spectra [3]. Such assumption is also made in the FABLES scheme for the retrieval of the internuclear separation [24].

In summary, we demonstrate a tomographic method to retrieve the molecular internuclear separation based on two-center interference with aligned diatomic molecules. Our measurement shows a prominent valley structure from the destructive two-center interference of the rescattered electrons in the alignment dependence of the high-energy photoelectron spectra along the laser polarization direction. Based on this two-center interference, we show that the detailed information about the molecular structure can be extracted, providing a more straightforward approach of molecular imaging based on strong-field ionization and rescattering, in comparison with LIED and FABLES schemes. Our tomographic method with the two-center interference of the aligned molecules may be applied to the more complex molecules, e.g., the multicenter molecules to retrieve the information of the molecular structure.

We thank Professor Jing Chen for stimulating discussions. This work is supported by the National Natural Science Foundation of China (No. 11834015, No. 11874392, No. 11804374, No. 11847243, No. 11774387, and No. 11527807), the Strategic Priority Research Program of the Chinese Academy of Sciences (No. XDB21010400), and the China Postdoctoral Science Foundation (Grant No. 2017M622557).

*xylai@wipm.ac.cn
†xjliu@wipm.ac.cn

[1] P. B. Corkum, Phys. Rev. Lett. **71**, 1994 (1993).
[2] K. J. Schafer, B. Yang, L. F. DiMauro, and K. C. Kulander, Phys. Rev. Lett. **70**, 1599 (1993).
[3] See, for example, W. Becker, F. Grasbon, R. Kopold, D. B. Milošević, G. G. Paulus, and H. Walther, Adv. At. Mol. Opt. Phys. **48**, 35 (2002); G. G. Paulus, W. Nicklich, H. Xu, P. Lambropoulos, and H. Walther, Phys. Rev. Lett. **72**, 2851 (1994); D. B. Milošević, G. G. Paulus, D. Bauer, and W. Becker, J. Phys. B **39**, R203 (2006).
[4] See, for example, M. Ferray, A. L'Huillier, X. F. Li, L. A. Lompré, G. Mainfray, and C. Manus, J. Phys. B **21**, L31 (1988); J. L. Krause, K. J. Schafer, and K. C. Kulander, Phys. Rev. Lett. **68**, 3535 (1992); P. Agostini and L. F. DiMauro, Rep. Prog. Phys. **67**, 813 (2004).
[5] B. Walker, B. Sheehy, L. F. DiMauro, P. Agostini, K. J. Schafer, and K. C. Kulander, Phys. Rev. Lett. **73**, 1227 (1994); A. Becker, R. Dörner, and R. Moshammer, J. Phys. B **38**, S753 (2005); W. Becker, X. J. Liu, P. J. Ho, and J. H. Eberly, Rev. Mod. Phys. **84**, 1011 (2012); C. F. de Morisson Faria and X. Liu, J. Mod. Opt. **58**, 1076 (2011).
[6] F. Krausz and M. Ivanov, Rev. Mod. Phys. **81**, 163 (2009).
[7] A. Talebpour, C.-Y. Chien, and S. L. Chin, J. Phys. B **29**, L677 (1996).
[8] C. Guo, M. Li, J. P. Nibarger, and G. N. Gibson, Phys. Rev. A **58**, R4271 (1998).
[9] J. Muth-Böhm, A. Becker, and F. H. M. Faisal, Phys. Rev. Lett. **85**, 2280 (2000).
[10] F. Grasbon, G. G. Paulus, S. L. Chin, H. Walther, J. Muth-Böhm, A. Becker, and F. H. M. Faisal, Phys. Rev. A **63**, 041402(R) (2001).
[11] Z. Y. Lin, X. Y. Jia, C. L. Wang, Z. L. Hu, H. P. Kang, W. Quan, X. Y. Lai, X. J. Liu, J. Chen, B. Zeng, W. Chu, J. P. Yao, Y. Cheng, and Z. Z. Xu, Phys. Rev. Lett. **108**, 223001 (2012).
[12] H. P. Kang, Z. Y. Lin, S. P. Xu, C. L. Wang, W. Quan, X. Y. Lai, X. J. Liu, X. Y. Jia, X. L. Hao, J. Chen, W. Chu, J. P. Yao, B. Zeng, Y. Cheng, and Z. Z. Xu, Phys. Rev. A **90**, 063426 (2014).
[13] M. Lein, N. Hay, R. Velotta, J. P. Marangos, and P. L. Knight, Phys. Rev. Lett. **88**, 183903 (2002).
[14] M. Lein, J. P. Marangos, and P. L. Knight, Phys. Rev. A **66**, 051404(R) (2002).
[15] T. Kanai, S. Minemoto, and H. Sakai, Nature (London) **435**, 470 (2005).
[16] C. Vozzi, F. Calegari, E. Benedetti, J.-P. Caumes, G. Sansone, S. Stagira, M. Nisoli, R. Torres, E. Heesel, N. Kajumba, J. P. Marangos, C. Altucci, and R. Velotta, Phys. Rev. Lett. **95**, 153902 (2005).
[17] P. Liu, P. F. Yu, Z. N. Zeng, H. Xiong, X. C. Ge, R. X. Li, and Z. Z. Xu, Phys. Rev. A **78**, 015802 (2008).
[18] M. Busuladžić, A. Gazibegović-Busuladžić, D. B. Milošević, and W. Becker, Phys. Rev. Lett. **100**, 203003 (2008).
[19] M. Busuladžić, A. Gazibegović-Busuladžić, D. B. Milošević, and W. Becker, Phys. Rev. A **78**, 033412 (2008).
[20] M. Okunishi, R. Itaya, K. Shimada, G. Prmper, K. Ueda, M. Busuladžić, A. Gazibegović-Busuladžić, D. B. Milošević, and W. Becker, Phys. Rev. Lett. **103**, 043001 (2009).
[21] T. Zuo, A. Bandrauk, and P. B. Corkum, Chem. Phys. Lett. **259**, 313 (1996).
[22] C. I. Blaga, J. L. Xu, A. D. DiChiara, E. Sistrunk, K. K. Zhang, P. Agostini, T. A. Miller, L. F. DiMauro, and C. D. Lin, Nature (London) **483**, 194 (2012).

[23] M. Meckel, D. Comtois, D. Zeidler, A. Staudte, D. Pavičić, H. C. Bandulet, H. Pépin, J. C. Kieffer, R. Dörner, D. M. Villeneuve, and P. B. Corkum, Science **320**, 1478 (2008).
[24] J. Xu, C. I. Blaga, K. Zhang, Y. H. Lai, C. D. Lin, T. A. Miller, P. Agostini, and L. F. DiMauro, Nat. Commun. **5**, 4635 (2014).
[25] M. G. Pullen, B. Wolter, A.-T. Le, M. Baudisch, M. Sclafani, H. Pires, C. D. Schröter, J. Ullrich, R. Moshammer, T. Pfeifer, C. D. Lin, and J. Biegert, Nat. Commun. **7**, 11922 (2016).
[26] R. Dörner, V. Mergel, O. Jagutzki, L. Spielberger, J. Ullrich, R. Moshammer, and H. Schmidt-Böcking, Phys. Rep. **330**, 95 (2000).
[27] J. Ullrich, R. Moshammer, A. Dorn, R. Dörner, L. Ph. H. Schmidt, and H. Schmidt-Böcking, Rep. Prog. Phys. **66**, 1463 (2003).
[28] For the details of our COLTRIMS setup, see e.g., Y. L. Wang, S. P. Xu, W. Quan, C. Gong, X. Y. Lai, S. L. Hu, M. Q. Liu, J. Chen, and X. J. Liu, Phys. Rev. A **94**, 053412 (2016); W. Quan, X. L. Hao, X. Q. Hu, R. P. Sun, Y. L. Wang, Y. J. Chen, S. G. Yu, S. P. Xu, Z. L. Xiao, X. Y. Lai, X. Y. Li, W. Becker, Y. Wu, J. G. Wang, X. J. Liu, and J. Chen, Phys. Rev. Lett. **119**, 243203 (2017).
[29] Because of the low frequency and long duration of the alignment pulse, the population of the excited vibrational wave packets of molecules is avoided and thus the molecular internuclear separation is hardly influenced by the alignment pulse; see, for example, H. Stapelfeldt and T. Seideman, Rev. Mod. Phys. **75**, 543 (2003); S. G. Walt, N. B. Ram, M. Atala, N. I. Shvetsov-Shilovski, A. von Conta, D. Baykusheva, M. Lein, and H. J. Wörner, Nat. Commun. **8**, 15651 (2017).
[30] P. W. Dooley, I. V. Litvinyuk, Kevin F. Lee, D. M. Rayner, M. Spanner, D. M. Villeneuve, and P. B. Corkum, Phys. Rev. A **68**, 023406 (2003).
[31] D. Pavičić, K. F. Lee, D. M. Rayner, P. B. Corkum, and D. M. Villeneuve, Phys. Rev. Lett. **98**, 243001 (2007).
[32] W. Quan, M. H. Yuan, S. G. Yu, S. P. Xu, Y. J. Chen, Y. L. Wang, R. P. Sun, Z. L. Xiao, C. Gong, L. Q. Hua, X. Y. Lai, X. J. Liu, and J. Chen, Opt. Express **24**, 23248 (2016).
[33] X. H. Xie, T. Wang, S. G. Yu, X. Y. Lai, S. Roither, D. Kartashov, A. Baltuška, X. J. Liu, A. Staudte, and M. Kitzler, Phys. Rev. Lett. **119**, 243201 (2017).
[34] D. B. Milošević and F. Ehlotzky, Adv. At. Mol. Opt. Phys. **49**, 373 (2003).
[35] G. G. Paulus, F. Grasbon, A. Dreischuh, H. Walther, R. Kopold, and W. Becker, Phys. Rev. Lett. **84**, 3791 (2000).
[36] H. Kang, W. Quan, Y. Wang, Z. Lin, M. Wu, H. Liu, X. Liu, B. B. Wang, H. J. Liu, Y. Q. Gu, X. Y. Jia, J. Liu, J. Chen, and Y. Cheng, Phys. Rev. Lett. **104**, 203001 (2010).
[37] P. E. Cade and A. C. Wahl, At. Data Nucl. Data Tables **13**, 339 (1974).
[38] P. W. Atkins and R. S. Friedman, *Molecular Quantum Mechanics*, 3rd ed. (Oxford University Press, Oxford, 2001).
[39] I. N. Levine, *Quantum Chemistry*, 5th ed. (Prentice-Hall, Upper Saddle River, NJ, 2000).
[40] R. Kopold, W. Becker, M. Kleber, and G. G. Paulus, J. Phys. B **35**, 217 (2002).
[41] M. Okunishi, H. Niikura, R. R. Lucchese, T. Morishita, and K. Ueda, Phys. Rev. Lett. **106**, 063001 (2011).
[42] M. G. Pullen, B. Wolter, A.-T. Le, M. Baudisch, M. Hemmer, A. Senftleben, C. D. Schröter, J. Ullrich, R. Moshammer, C. D. Lin, and J. Biegert, Nat. Commun. **6**, 7262 (2015).